by applying the method by the reference (Kohri et al., 2001) for five subjects whose absorption coefficients (μ_a) increased proportional to optode spacing from 2 to 4 cm. The observed mean pathlength (L_{obs}) was calculated (Zhang et al., 1998) from temporal profiles. Then, we determined the contribution ratio of the intracerebral tissue to the observed absorption change using these values.

TRS fiber position

Prior to the experiment, headgear was made for each volunteer to fix the TRS optical fibers to their left forehead. The headgear was made of thermoplastic material (ESS-15, Engineering System Co., Japan) to ensure a secure fit onto the head of each volunteer. A total of five fiber holders were fabricated for four light irradiation points (S_{1-4}) with optode spacings of 2, 3, 4 and 5 cm and one light detection point (D), and a black sheet was affixed to the inner side of the headgear except for the fiber holders to shield a detection fiber from stray light propagating on the skin surface. More specifically, the light irradiation point S_4 was first established on the left forehead, at a point 35 mm above supra-orbital margin so as to avoid the frontal sinus, and also 1 cm away from the median line to avoid the superior sagittal sinus. Next, the other light irradiation and detection points (S_{1-3}, D) were established using this point (S_4) as a reference. The positions of the light irradiation and detection points (S_{1-4}, D) on the MRI image of the head are shown in Fig. 2A. After measurement was complete, the value of optode spacing for substitution into the photon diffusion equation was measured as a straight distance with calipers. Fabricating headgear allowed the measurement to be easily made and permitted setting accurate optode spacing.

PET procedure

PET was performed using a high resolution PET scanner (SHR22000, Hamamatsu Photonics KK, Hamamatsu, Japan) (Iwase et al., 2002) with spatial resolution of 3.6 mm at full width half maximum (FWHM) transaxially and 4.2 mm axially, and with a 23-cm axial field of view, yielding 63 image slices simultaneously. After backprojection and filtering, the image resolution was 8.0 × 8.0 × 5.3 mm FWHM. The voxel of each reconstructed image measured 1.73 × 1.73 × 3.6 mm. Just prior to PET measurement, each subject underwent an MRI for determining the brain scanning area by using a static magnet with 3-dimensional mode acquisition (Ouchi et al., 1998). Fifteen-minute transmission scan for attenuation correction was performed with a $^{68}Ge/^{68}Ga$ source.

We applied the ^{15}O-CO short inhalation method followed by 5 min of data acquisition to measure the PET CBV (Lammertsma and Jones, 1983; Lammertsma et al., 1987). During this acquisition period, two pairs of arterial blood samples were collected for determining arterial ^{15}O-CO radioactivity.

One hundred twenty-second dynamic emission scans (10 s × 12 frames) were performed while subjects received a 500-MBq bolus of $H_2^{15}O$ through the right cubital vein by an automated injector. Simultaneously after injection, arterial blood was continuously withdrawn through the left brachial artery using the automated arterial blood γ-ray coincidence counter (BACC-2: Hamamatsu Photonics K.K., Hamamatsu, Japan) yielding arterial input data per second (Ouchi et al., 2001). A quantitative PET CBF value was estimated using 2-min $H_2^{15}O$ data accumulated after the tracer started circulating in the brain by summing the dynamic frames based on the autoradiographic method (Herscovitch et al., 1983).

Physiological parameters were monitored during PET examination and additional arterial blood samples were taken after each scan for analyzing levels of $PaCO_2$, Hb, hematocrit and arterial pH using a blood gas analyzer (Bayer Rapidlab 860, Tokyo, Japan). The psychophysical condition of each subject was evaluated by asking if any different sensation or mental activity was developed during the whole measurement in order to exclude any change in such brain activities as a confounding factor.

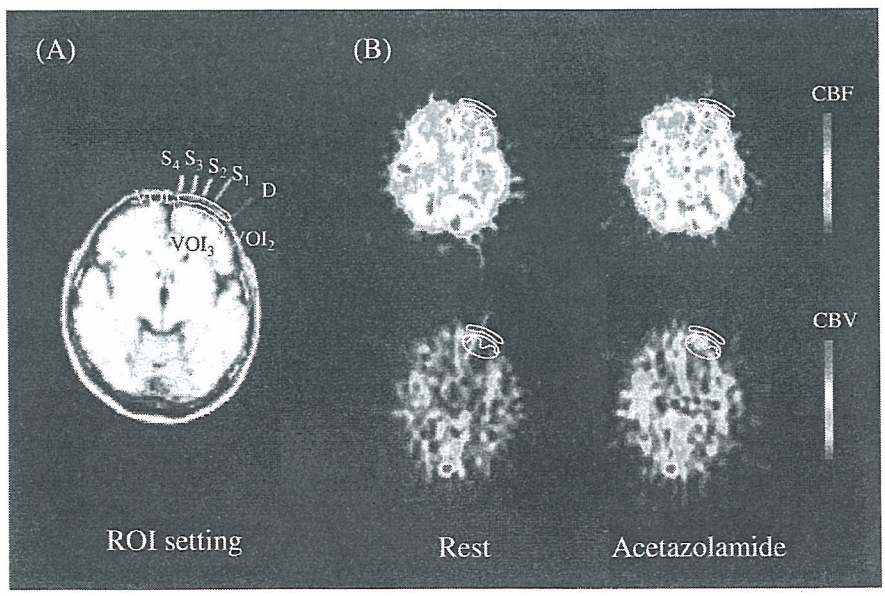

Fig. 2. Fiber and VOI positions setting on MRI image and PET images. (A) Fiber markers appear on left forehead. S_{1-4} and D are corresponding to irradiation fibers and a detection fiber, respectively. Optode spacings of S_1-D: 2 cm, S_2-D: 3 cm, S_3-D: 4 cm, S_4-D: 5 cm were set. The four PET VOIs were set as follows. VOI_1: extracerebral tissue, VOI_2: gray matter region, VOI_3: gray matter and white matter regions. (B) Images of typical measurements (41 years old; male) of PET CBF (upper) and PET CBV (lower) in the resting (left) and loading (right) state.

After measurements, to grasp the TRS light irradiation and detection points on the PET image, the fiber positions were marked by multi-modality radiographic markers (MM-3004, I.Z.I Medical Products Corp., USA) and the brain once again measured by MRI.

PET VOI

The volume of interest (VOI) on PET image used for comparison with TRS values was set by means of the following procedure. First of all, 3-dimensional MRI images were cut into 3.6 mm thick slices transversely along the multi-modality radiographic marker line. Then two slices involving these markers were selected from all these slices. Next, the following four VOIs were placed under S_4-D area on the two slices. These were set as VOI_1: extracerebral tissues (such as scalp and skull), VOI_2: gray matter region, VOI_3: gray matter and white matter regions. These VOIs were then repositioned on the PET image matching the selected two MRI slices as the PET VOIs. Mean values for each VOI size were VOI_1: 2.88 cm^3, VOI_2: 3.16 cm^3, VOI_3: 5.99 cm^3. The VOI settings are shown in Fig. 2A.

Since the PET CBF and PET CBV values were calculated with coefficients established for intracerebral tissues, the data of VOI_1 set in extracerebral tissues were treated with arbitrary unit.

Protocol

PET measurements were performed in the resting state (before administration) and the loading state (after administration) at more than 20 min after the intravenous administration of 1000 mg acetazolamide (Diamox, Japan Wyeth Ledele Ltd., Japan) appeared to be the maximum effect of cerebral vasodilatation. Two CBF measurements and one CBV measurement with PET were performed in resting and loading state.

In the TRS measurement, the optode spacings were changed in sequence by switching the four light irradiation points (S_{1-4}) with an optical switch. To maintain a peak count greater than 5000 (Suzuki et al., 1994), the acquisition times at each light irradiation point were set to 10, 20, 30 and 120 s. These TRS measurements were performed consecutively on a time series from the start to the finish of the PET measurements. Subjects were kept at rest while lying face up on the bed during measurements. The protocol is shown in Fig. 3.

Statistical analysis

All results were expressed as mean ± SD. Statistical significance of the changes in PET CBV, PET CBF, TRS CBV and SO_2 before and after administration of acetazolamide was analyzed by paired t test. Statistical significance of contribution ratio among wavelengths was analyzed by ANOVA and Bonferroni t test. A significant difference was defined when statistical probability: P was less than 0.05.

The association between TRS CBV and PET CBV was evaluated by squared Pearson's correlation coefficient (r^2). Change in CBV (ΔCBV) by administration of acetazolamide was also evaluated in the same way. The assessment for VOI_1 was not performed because it was expressed in the arbitrary unit. Statistical significance of r^2 was analyzed by a t test for r^2. A significant difference was defined when statistical probability: P was less than 0.05.

Results

Physiology

There were no significant changes in physiologic parameters (arterial blood pressure, pulse rates, $PaCO_2$) and psychophysical states (changes in mental activity) between before and after administration of acetazolamide (data is not shown).

TRS

Typical values of TRS tHb and SO_2 at each optode spacing during the experiment are shown in Fig. 4. The rise of TRS tHb and SO_2 was confirmed at all optode spacings immediately after administering acetazolamide and reached a plateau after about 10 min. These phenomena were observed in all subjects.

Mean values of TRS CBV and SO_2 at each optode spacing in the resting and loading states are shown in Fig. 5. The TRS CBV and SO_2 at each optode spacing in resting state were as follows: 2 cm: 2.7 ± 0.4 cm^3/100 g, 70.3 ± 1.1%, 3 cm: 3.0 ± 0.2 cm^3/100 g, 68.7 ± 1.8%, 4 cm: 3.0 ± 0.3 cm^3/100 g, 69.6 ± 2.3%, 5 cm: 2.7 ± 0.3 cm^3/100 g, 71.7 ± 2.8%. The TRS CBV and SO_2 in loading

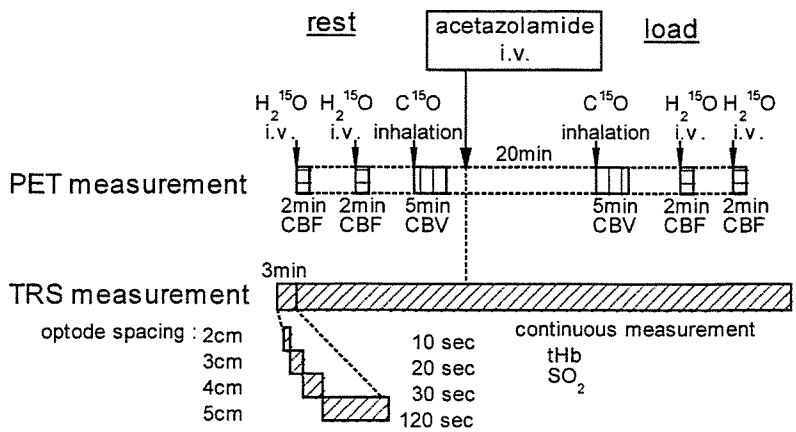

Fig. 3. TRS and PET simultaneous measurement protocol. The TRS measurement was made while switching the light irradiation point to set optode spacings of 2, 3, 4 and 5 cm. Data acquisition time was 10, 20, 30 and 120 s at each irradiation point. In the PET measurement, CBF was measured twice and CBV once, both resting and loading state. One CBF measurement required 2 min and the CBV measurement 5 min.

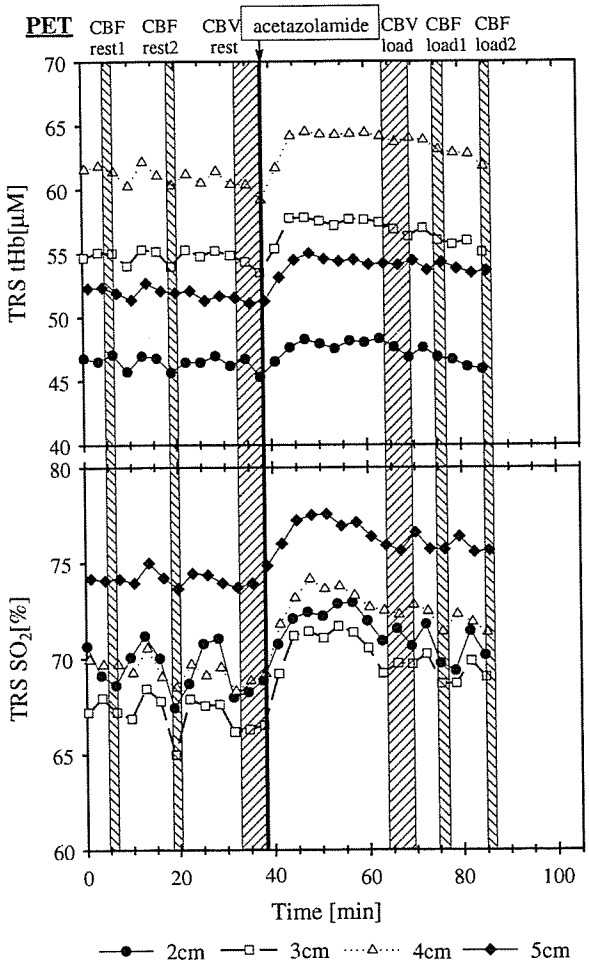

Fig. 4. TRS measurement results at each optode spacing. Typical responses (41 years old; male) of TRS tHb (upper) and SO_2 (lower) for acetazolamide administration. The oblique lines indicate PET data acquisition period.

state significantly rose approximately 6% and 3%, respectively, of resting state at all optode spacing.

PET

The CBF and CBV images at the resting and loading state are shown in Fig. 2B. The CBF can be clearly seen to increase after administering acetazolamide, whereas the CBV shows a relatively minor increase.

Mean values of PET CBF and PET CBV at each VOI in the rest and loading state are shown in Fig. 6. The PET CBF and PET CBV at each VOI in the resting state were as follows: VOI_1 (arbitrary unit): 6.6 ± 1.2 cm^3/100 g/min, 2.6 ± 0.4 cm^3/100 g, VOI_2: 39.6 ± 5.3 cm^3/100 g/min, 4.4 ± 0.9 cm^3/100 g, VOI_3: 40.6 ± 5.1 cm^3/100 g/min, 4.0 ± 0.7 cm^3/100 g. The PET CBF and PET CBV at $VOI_{2,3}$ in the loading state significantly increased approximately 30% and 10%, respectively, compared to those of resting state. However, no significant increases were observed for the CBF and CBV at VOI_1, which increased 8.2% and −1.3%, respectively.

Correlations

The r^2 for the CBV and ΔCBV, respectively, between TRS and PET are shown in Tables 1A and B.

The r^2 of CBV at 4 cm and 5 cm of optode spacing was higher than those at 2 cm and 3 cm of optode spacing at all VOI, and they also showed high correlation values as the depth increased.

As to ΔCBV, r^2 of VOI_2 showed exceptionally higher than those of VOI_3 at all optode spacing. At the VOI_2, however, r^2 at 2 cm of optode spacing showed lower than those at other optode spacing. At the VOI_3, just as with the CBV correlation, r^2 at 4 cm and 5 cm of optode spacing showed higher than those at 2 cm and 3 cm of optode spacing.

L_{ext} and the contribution ratio

L_{ext} at each wavelength was as follows: 761 nm 11.7 ± 2.7 cm, 791 nm: 6.3 ± 2.4 cm, 836 nm: 6.5 ± 1.5 cm. L_{ext} at 761 nm was significantly longer than those of 791 and 836 nm, against

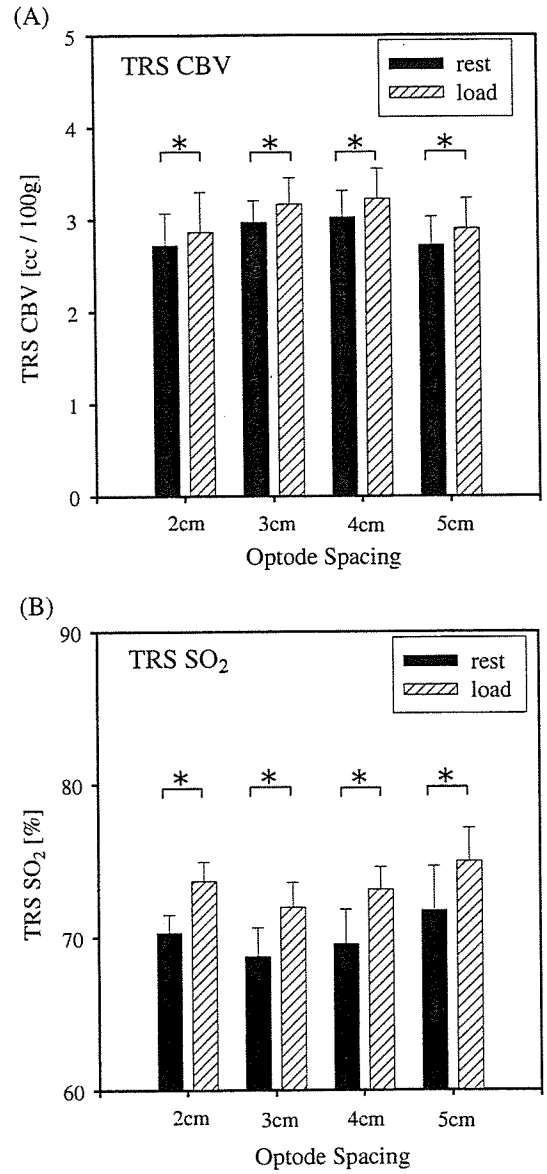

Fig. 5. Mean values (n = 6) for (A) TRS CBV and (B) SO_2 in the resting and loading state. Significant differences were confirmed for all optode spacings after administering acetazolamide (*P < 0.05).

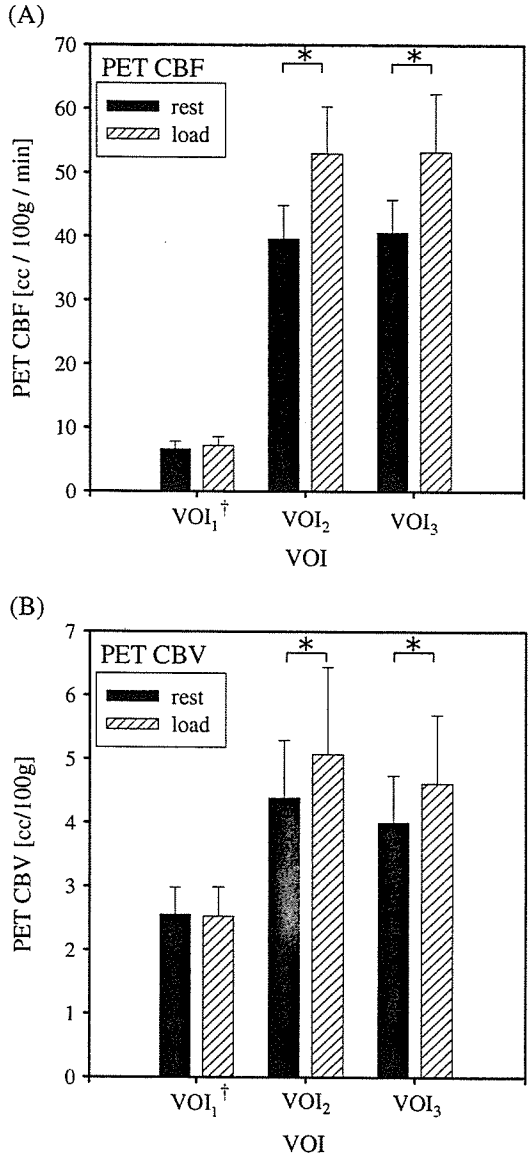

Fig. 6. Mean values (n = 6) for (A) PET CBF and (B) PET CBV in the resting and loading state. Significant differences were confirmed at VOI_2 and VOI_3 after administering acetazolamide (*P < 0.05). †VOI_1 was expressed in the arbitrary unit.

observed mean pathlength of each wavelengths were also the same (data is not shown).

The contribution ratios of the cerebral tissue at each wavelength are shown in Fig. 7. The contribution ratios of 761 nm with all optode spacing were significantly lower than those of 791 and 836 nm.

Discussion

The acetazolamide used in this experiment increases the regional CBF by inhibiting carbonic anhydrase and thereby expanding cerebral blood vessels (Posner and Plum, 1960; Ehrenreich et al., 1961). This drug is therefore generally used to assess the cerebrovascular reserve capacity as an acetazolamide test. Similarly in this study, significant increases of PET CBF and PET CBV by

Table 1
Squared correlation coefficient (r^2) between PET and TRS: (A) CBV; (B) ΔCBV

TRS optode spacing	PET	
	VOI_2	VOI_3
(A) r^2: TRS CBV vs. PET CBV (n = 6)		
2 cm	0.601**	0.535**
3 cm	0.410*	0.525**
4 cm	0.690**	0.841**
5 cm	0.762**	0.859**
(B) r^2: TRS ΔCBV vs. PET ΔCBV (n = 6)		
2 cm	0.331	0.050
3 cm	0.633*	0.277
4 cm	0.699*	0.457
5 cm	0.585	0.352

* $P < 0.05$.
** $P < 0.01$.

acetazolamide in the intracerebral tissues ($VOI_{2,3}$) and no significant increase of those in the extracerebral tissues (VOI_1) were confirmed. In the TRS measurements on the other hand, significant increases in CBV at all optode spacings were observed. Further, the result of significant increases of SO_2 at all optode spacing agrees well with a report (Vorstrup et al., 1984) that there was hardly any change in $CMRO_2$ even though the CBF increased when acetazolamide was administered. These results suggest that when optode spacing is 2 cm to 5 cm, the photons passing through the head convey the intracerebral hemodynamic response.

However, the CBV and ΔCBV correlations clearly differed according to the optode spacing and VOI. As for CBV correlation, these trends suggest that the longer the optode spacing, the deeper the region that the photons can penetrate, because the correlation with VOI_3 was higher than that with VOI_2 at each optode spacing except at 2 cm. In addition, correlations at 4 cm and 5 cm of optode spacing showed a trend to higher than those at 2 cm and 3 cm of optode spacing with both VOIs. These results suggested that optode spacing was preferably more than 4 cm for improving quantification of NIR-TRS to cerebral hemodynamics.

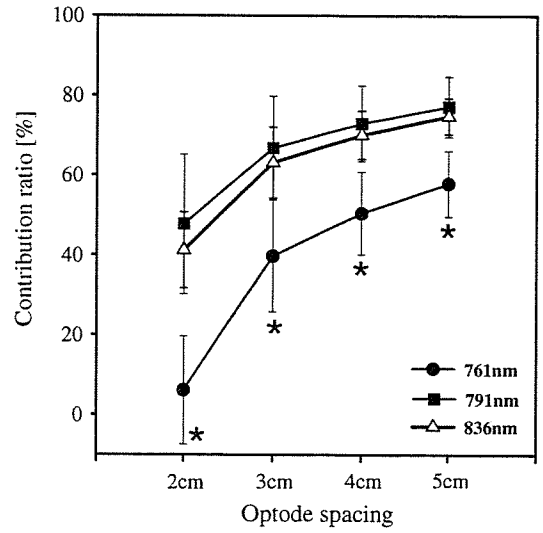

Fig. 7. Mean values (n = 5) for contribution rations of the cerebral tissue to observed absorption change. Significant differences were confirmed for all optode spacing at 761 nm to 791 and 836 nm (*P < 0.05).

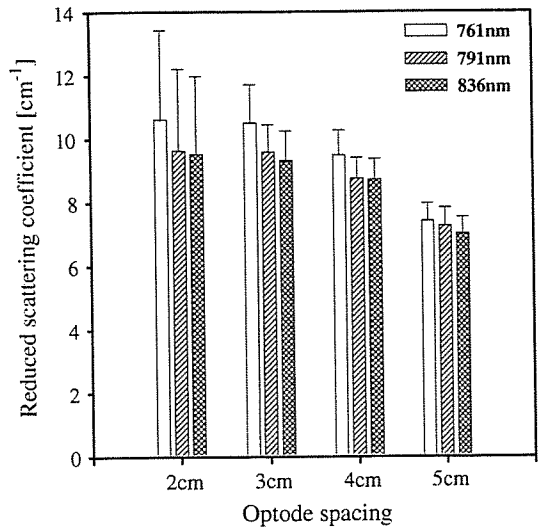

Fig. 8. Mean values (n = 5) for reduced scattering coefficient at each wavelength and optode spacing. The values of 761 nm for all optode spacing were highest among three wavelengths (no significant differences).

Because the density of blood vessels in VOI_2, which covers the gray matter mostly, was high, there might be a large increase in blood volume. Accordingly, the ΔCBV correlation with VOI_2 may be higher than VOI_3 regardless of the optode spacing. Also, the ΔCBV correlation for VOI_2 is a maximum at 4 cm of optode spacing so that this distance may be optimum for capturing cerebral hemodynamics response around the gray matter region.

Contribution ratios at 4 cm of optode spacing were as follows: 761 nm: 50.4 ± 10.3%, 791 nm: 72.9 ± 9.4%, 836 nm: 70.0 ± 6.0%. The results at 836 nm are very much in agreement with the results at 834 nm by Kohri (Kohri et al., 2001). But these results are different from previous simulation work (Firbank et al., 1995). The photon propagation depends heavily on the optical parameters of tissues. We believe that the μ_a and μ_s' of the postmortem adult human brain (Van der Zee et al., 1992) and piglet (Firbank et al., 1993) used in the simulation work maybe different from those in living tissues. Furthermore, both contribution ratios at 5 cm of optode spacing were higher than those at 4 cm and the ΔCBV correlation at 5 cm of optode spacing is lower than that at 4 cm; thus it is speculated that photons has penetrated even deeper, and contains information not only on gray matter but also on white matter and cerebral ventricle. Conversely, the lowest value of the ΔCBV correlation at 2 cm of optode spacing corresponds with derived low contribution ratios. So the 2 cm of optode spacing is not recommended for acquiring intracerebral information. Although we treated a complex layered structure as a single set of μ_a and μ_s', assuming of a homogeneous medium, making optode spacing longer could satisfy this condition concededly.

L_{ext} at 761 nm was 1.7 times of those at 791 and 836 nm, although observed mean pathlength at each wavelength was also the same values. It means that the photons of 761 nm are hard to penetrate into the cerebral tissue than those of 791 and 836 nm. To support this result, mean values for μ_s' at each wavelength and the optode spacing in the resting state are shown in Fig. 8. As the higher the scattering, the photons are harder to spread into the cerebral tissue deeply. The difference of μ_s' among wavelength showed a similar tendency to that of L_{ext}. It was also reported that the value of μ_s' increases progressively with decreasing wavelength (Bevilacqua et al., 1999; Torricelli et al., 2001). To improve the accuracy of NIR measurement, it should be necessary to consider wavelength selection including μ_s' as well as absorption spectra of hemoglobin.

The TRS system has a potential to quantitate the hemoglobin concentration since it directly measures the optical pathlength distribution of detected photons passing through the living tissue, different from the conventional measurement methods (Brazy et al., 1985; Ferrari et al., 1987; Cope and Delpy, 1988). This allows making patient-to-patient comparisons and comparing the patient condition before and after treatment, making it highly valuable as an indicator for diagnosis and treatment. In this study, a good correlation coefficient was obtained between TRS-derived CBV and PET-derived CBV, while the absolute CBV levels by TRS were lower than those by PET. One reason for the under-/over-estimation of the CBV values might be a difference in modalities which measure different in vivo responses. An absolute value of CBV weighs considerably in the NIRS study. Thus, further studies are needed to resolve this methodological issue.

NIR measurement is proven capable of continuous measurement with high time resolution while also being a simple, safe and non-invasive method. Additionally, study of diffuse optical tomography is being proceeded based on this technology (Ueda et al., 2001; Hillman et al., 2001). We hope to further develop our work in the NIRS field to the level where it can be used as a modality to assist and complement PET technology.

Conclusion

We observed a change in the CBV by administration of acetazolamide with simultaneous measurement of TRS and PET. These experiments showed that intracerebral hemodynamics response by administering acetazolamide could be captured at optode spacings of 2 cm to 5 cm.

Furthermore, by evaluating the correlation with PET, we concluded that more than 4 cm of optode spacing is preferable for improving quantification of the NIR-TRS measurement to intracerebral hemodynamics. Additionally, 4 cm of optode spacing is a good setting to monitor cerebral hemodynamics response around the gray matter region. Contribution ratio of intracerebral tissue at 4 cm estimated about 70%, although it varies according to wavelength. NIR measurement is a simple and easy method to evaluate cerebral hemodynamics.

Acknowledgments

The authors would like to thank Mr. T. Hiruma for his constant support and encouragement. The authors are also grateful to Drs. Y. Tsuchiya and T. Yamashita for useful discussions.

Appendix A. Derive reduced scattering and absorption coefficients from temporal profiles

Behavior of photon within scattering and absorption media like a living body is expressed by the photon diffusion Eq. (1) (Patterson et al., 1989).

$$\frac{1}{v}\frac{\partial}{\partial t}\phi(r,t) - D\nabla^2\phi(r,t) + \mu_a\varphi(r,t) = S(r,t) \quad (1)$$

where $\phi(r, t)$ is the diffuse photon fluence rate at position r and time t, D is the photon diffusion coefficient and expressed in $D = 1/3\mu_s'$, v is the velocity of light within the media and $S(r, t)$ is the light source.

Solutions using this equation are found under different boundary conditions. We used the solution of a semi-infinite homogeneous model (Patterson et al., 1989) for TRS data analysis. In this solution, $R(d, t)$ is expressed by a function of the optode spacing, the reduced scattering coefficient (μ_s') and absorption coefficient (μ_a), as shown in Eq. (2).

$$R(d,t) = (4\pi Dv)^{-\frac{3}{2}} z_0 t^{-\frac{5}{2}} \exp(-\mu_a vt) \exp\left(-\frac{d^2 + z_0^2}{4Dvt}\right) \tag{2}$$

where d is the optode spacing and $z_0 = 1/\mu_s'$.

Using the non-linear least squares method, we fit Eq. (2) into the observed temporal profiles obtained from TRS and determined μ_s' and μ_a at each wavelength (Suzuki et al., 1994). The conversion chi-square (χ_v^2) value was adopted to evaluate fitting accuracy. We confirmed that our observed profiles fitted well with the theoretical curves using this index ($0.8 < \chi_v^2 < 1.2$; Grinvald and Steinberg, 1974).

Appendix B. Calculation of hemoglobin concentration and oxygen saturation by absorption coefficients

The μ_a of the 3 wavelengths (761, 791, 836 nm) that were measured is expressed as shown in simultaneous Eq. (3).

$$\begin{aligned}
\mu_{a761nm} &= \varepsilon_{oxyHb761nm} C_{oxyHb} + \varepsilon_{deoxyHb761nm} C_{deoxyHb} \\
&\quad + \varepsilon_{H_2O761nm} C_{H_2O} + \mu_{abkg761nm} \\
\mu_{a791nm} &= \varepsilon_{oxyHb791nm} C_{oxyHb} + \varepsilon_{deoxyHb791nm} C_{deoxyHb} \\
&\quad + \varepsilon_{H_2O791nm} C_{H_2O} + \mu_{abkg791nm} \\
\mu_{a836nm} &= \varepsilon_{oxyHb836nm} C_{oxyHb} + \varepsilon_{deoxyHb836nm} C_{deoxyHb} \\
&\quad + \varepsilon_{H_2O836nm} C_{H_2O} + \mu_{abkg836nm}
\end{aligned} \tag{3}$$

where μ_a is the absorption coefficient at the wavelength λ, $\varepsilon_{m\lambda}$ is the molar extinction coefficient of the substance m at the wavelength λ, C_m is the concentration of the substance m and bkg is the chromophores contributing to μ_a in tissue for other than oxygenated hemoglobin (oxyHb), deoxygenated hemoglobin (deoxyHb) and water.

Based on the assumption that light absorption in the living body in this wavelength region occurs from oxyHb, deoxyHb and water, and also that there is no other background absorption in the living body (Tromberg et al., 1997), we determined TRS values for oxygenated hemoglobin (TRS HbO_2) and deoxygenated hemoglobin (TRS Hb) as tissue water concentration is 70%.

TRS total hemoglobin (TRS tHb) and SO_2 were obtained from Eq. (4) as follows.

$$\text{TRS tHb}[\mu M] = \text{TRS HbO}_2 + \text{TRS Hb},$$

$$SO_2[\%] = \frac{\text{TRS HbO}_2}{\text{TRS tHb}} \times 100 \tag{4}$$

Appendix C. Conversion TRS tHb into TRS CBV

We converted the TRS tHb into the CBV by TRS (TRS CBV) using Eq. (5) (Wyatt et al., 1990) for comparison with the CBV by PET (PET CBV).

$$\text{TRS CBV}[\text{cc}/100\text{ g}] = \frac{\text{TRS tHb} \times \text{MW}_{Hb}}{\text{Hb} \times \eta \times \rho \times 100000} \tag{5}$$

where MW_{Hb} is hemoglobin molecular weight; 64,500, Hb is arterial hemoglobin concentration (g/dl) of subject, η is the cerebral-to-large-vessel hematocrit ratio; 0.85 (Phelps et al., 1979) and ρ is density of cerebral tissue (g/ml); 1.04 (Picozzi et al., 1985).

References

Bevilacqua, F., Piguet, D., Marquet, P., Gross, J.D., Tromberg, B.J., Depeursinge, C., 1999. In vivo local determination of tissue optical properties: applications to human brain. Appl. Opt. 38 (22), 4839–4950.

Brazy, J.E., Lewis, D.V., Mitnick, M.H., Jobsis, F.F., 1985. Noninvasive monitoring of cerebral oxygenation in preterm infants: preliminary observations. Pediatrics 75, 217–225.

Cope, M., Delpy, D.T., 1988. A system for long-term measurement of cerebral blood and tissue oxygenation in newborn infants by near infrared transillumination. Med. Biol. Eng. Comput. 26, 289–294.

De Blasi, R.A., Almenräder, N., Ferrari, M., 1997. Brain oxygenation monitoring during cardiopulmonary bypass by near infrared spectroscopy. Adv. Exp. Med. Biol. 413, 97–104.

Ehrenreich, D.L., Burns, R.A., Alman, R.W., Fazekas, J.F., 1961. Influence of acetazolamide on cerebral blood flow. Arch. Neurol. 5, 227–232.

Ferrari, M., Zanette, E., Sideri, G., Gianni, I., Fieschi, C., Carpi, A., 1987. Effects of carotid compression, as assessed by near infrared spectroscopy, upon cerebral volume and haemoglobin oxygen saturation. J. R. Soc. Med. 80, 83–87.

Firbank, M., Hiraoka, M., Essebpreis, M., Delpy, D.T., 1993. Measurement of the optical properties of the skull in the wavelength range 650–950 nm. Phys. Med. Biol. 38, 503–510.

Firbank, M., Schweiger, M., Delpy, D.T., 1995. Investigation of 'light piping' through clear regions of scattering objects. SPIE 2389, 167–173.

Germon, T.J., Evans, P., Barnett, N., Wall, P., Nelson, R.J., 1995. Optode separation determines sensitivity of near infrared spectroscopy to intra- and -external oxygenation changes. J. Cereb. Blood Flow Metab. 15, 617.

Grinvald, A., Steinberg, I.Z., 1974. On the analysis of fluorescence decay kinetics by the method of least-squares. Anal. Biochem. 59 (5), 583–598.

Harris, D.N.F., Cowans, F.M., Wertheim, D.A., Hamid, S., 1994. NIRS in adult-effects of increasing optode separation. Adv. Exp. Med. Biol. 345, 837–840.

Herscovitch, P., Markham, J., Raichle, M.E., 1983. Brain blood flow measured with intravenous H215O: I. Theory and error analysis. J. Nucl. Med. 24, 782–789.

Hillman, E., Hebden, J., Schweiger, M., Dehghani, H., Schmidt, F.E.W., Delpy, D.T., Arridge, S.R., 2001. Time resolved optical tomography of the human forearm. Phys. Med. Biol. 46, 1117–1130.

Isobe, K., Kusaka, T., Fujikawa, Y., Kondo, M., Yasuda, S., Itoh, S., Hirano, K., Onishi, S., 2000. Changes in cerebral hemoglobin concentration and oxygen saturation immediately after birth in the human neonate using full-spectrum near infrared spectroscopy. J. Biomed. Opt. 5 (3), 283–286.

Iwai, H., Urakami, T., Miwa, M., Nishizawa, M., Tsuchiya, Y., 2001. Tissue spectroscopy with a newly developed phase modulation system based on the microscopic Beer-Lambert law. SPIE 4250, 482–488.

Iwase, M., Ouchi, Y., Okada, H., Yokoyama, C., Nobezawa, S., Yoshikawa, E., Tsukada, H., Takeda, M., Yamashita, K., Takeda, M., Yamaguti, K., Kuratsune, H., Shimizu, A., Watanabe, Y., 2002. Neural substrates of human facial expression of pleasant emotion induced by comic films: a PET study. NeuroImage 17, 758–768.

Jobsis, F.F., 1977. Noninvasive, infrared monitoring of cerebral and myocardial oxygen sufficiency and circulatory parameters. Science 198, 1264–1267.

Kakihana, Y., Matsunaga, A., Yamada, H., Dohgomori, H., Oda, T., Yoshimura, N., 1996. Continuous, noninvasive measurement of cytochrome oxidase in cerebral cortex by near-infrared spectrophotometry during aortic arch surgery. J. Anesth. 10, 221–224.

Kohri, S., Hoshi, Y., Tamura, M., Kato, C., Kuge, Y., Tamaki, N., 2001. Quantitative evaluation of the relative contribution ratio of cerebral tissue to near-infrared signals in adult human head. A preliminary study. Physiol. Meas. 23 (2), 301–312.

Lammertsma, A.A., Jones, T., 1983. Correction for the presence of intravascular oxygen-15 in the steady-state technique for measuring regional oxygen extraction ratio in the brain: 1. Description of the method. J. Cereb. Blood Flow Metab. 3, 416–424.

Lammertsma, A.A., Baron, J.C., Jones, T., 1987. Correction for intravascular activity in the oxygen-15 steady-state technique is independent of the regional hematocrit. J. Cereb. Blood Flow Metab. 7, 372–374.

McCormick, P.W., Stewart, M., Lewis, G., Dujovny, M., Ausman, J.I., 1992. Intracerebral penetration of infrared light. J. Neurosurg. 76 (2), 315–319.

Meek, J.H., Elwell, C.E., McCormick, D.C., Edwards, A.D., Townsend, J.P., Stewart, A.L., Wyatt, J.S., 1999. Abnormal cerebral haemodynamics in perinatally asphyxiated neonates related to outcome. Arch. Dis. Child., Fetal Neonatal Ed. 81 (2), F110–F115 (Sep).

Misonoo, S., Okada, E., 2001. Adult head modeling based on time-resolved measurement for NIR instrument. SPIE 4250, 522–529.

Oda, M., Yamashita, Y., Nishimura, G., Tamura, M., 1996. A simple and novel algorithm for time-resolved multiwavelength oximetry. Phys. Med. Biol. 41, 551–562.

Oda, M., Nakano, T., Suzuki, A., Shimizu, K., Hirano, I., Shimomura, F., Ohmae, E., Suzuki, T., Yamashita, Y., 2000. Nearinfrared time-resolved spectroscopy system for tissue oxygenation monitor. SPIE 4160, 204–210.

Okada, E., Delpy, D.T., 2000. Effects of scattering of arachnoid trabeculae on light propagation in the adult brain. Advances in optical imaging, photon migration, and tissue optics. OSA Tech. Dig. 256–258.

Okada, E., Delpy, D.T., 2003a. Near-infrared light propagation in an adult head model: I. Modeling of low-level scattering in the cerebrospinal fluid layer. Appl. Opt. 42 (16), 2906–2914.

Okada, E., Delpy, D.T., 2003b. Near-infrared light propagation in an adult head model: II. Effect of superficial tissue thickness on the sensitivity of the near-infrared spectroscopy signal. Appl. Opt. 42 (16), 2915–2922.

Okada, E., Firbank, M., Schweiger, M., Arridge, S.R., Cope, M., Delpy, D.T., 1997. Theoretical and experimental investigation of near-infrared light propagation in a model of the adult head. Appl. Opt. 36 (1), 21–31.

Ouchi, Y., Nobezawa, S., Okada, H., Yoshikawa, E., Futatsubashi, M., Kaneko, M., 1998. Altered glucose metabolism in the hippocampal head in memory impairment. Neurology 51, 136–142.

Ouchi, Y., Okada, H., Yoshikawa, E., Futatsubashi, M., Nobezawa, S., 2001. Absolute changes in regional cerebral blood flow in association with upright posture in humans: an orthostatic PET study. J. Nucl. Med. 42, 707–712.

Patterson, M.S., Chance, B., Wilson, B.C., 1989. Time resolved reflectance and transmittance for the noninvasive measurement of tissue optical properties. Appl. Opt. 28 (12), 2331–2336.

Phelps, M.E., Huang, S.C., Hoffman, E.J., Kuhl, D.E., 1979. Validation of tomographic measurement of cerebral blood volume with C-11-labeled carboxyhemoglobin. J. Nucl. Med. 20, 328–334.

Picozzi, P., Todd, N.V., Crockard, A.H., 1985. The role of cerebral blood volume changes in brain specific-gravity measurements. J. Neurosurg. 62 (5), 704–710 (May).

Posner, J.P., Plum, F., 1960. The toxic effects of carbon dioxide and acetazolamide in hepatic encephalopathy. J. Clin. Invest. 39, 1246–1258.

Suzuki, K., Yamashita, Y., Ohta, K., Chance, B., 1994. Quantitative measurement of optical parameters in the breast using time-resolved spectroscopy. Invest. Radiol. 29 (4), 410–414.

Suzuki, S., Takasaki, S., Ozaki, T., Kobayashi, Y., 1999. A tissue oxygenation monitor using NIR spatially resolves spectroscopy. SPIE 3597, 582–592.

Tanosaki, M., Hoshi, Y., Iguchi, Y., Oikawa, Y., Oda, I., Oda, M., 2001. Variation of temporal characteristics in human cerebral hemodynamic responses to electric median nerve stimulation: a near-infrared spectroscopic study. Neurosci. Lett. 316, 75–78.

Torricelli, A., Pifferi, A., Taroni, P., Giambattistelli, E., Cubeddu, R., 2001. In vivo optical characterization of human tissues from 610 to 1010 nm by time-resolved reflectance spectroscopy. Phys. Med. Biol. 46, 2227–2237.

Tromberg, B.J., Coquoz, O., Fishkin, J.B., Pham, T., Anderson, E., Butler, J., Cahn, M., Gross, J.D., Venugopalan, V., Pham, D., 1997. Non-invasive measurements of breast tissue optical properties using frequency-domain photon migration. Philos. Trans. R. Soc. Lond., B 352, 661–668.

Tuchiya, Y., Urakami, T., 1996. Frequency domain analysis of photon migration based on the microscopic Beer-Lambert law. Jpn. J. Appl. Phys. 35, 4848–4851.

Ueda, U., Ohta, K., Oda, M., Miwa, M., Tsuchiya, Y., Yamashita, Y., 2001. 3-D imaging of a tissue-like phantom by diffusion optical tomography. Appl. Opt. 40 (34), 6349–6355.

Van der Zee, P., Cope, M., Arridge, S.R., Essenpreis, M., Potter, L.A., Edwards, A.D., Wyatt, J.S., McCormick, D.C., Roth, S.C., Reynolds, E.O.R., Delpy, D.T., 1992. Experimentally measured optical pathlength for the adult head, calf and forearm and the head of the newborn infant as a function of inter optode spacing. Exp. Med. Biol. 316, 143–153.

Vorstrup, S., Henriksen, L., Paulson, O., 1984. Effect of acetazolamide on cerebral blood flow and cerebral metabolic rate for oxygen. J. Clic. Invest. 74, 1634–1639.

Watanabe, E., Maki, A., Kawaguchi, F., Yamashita, Y., Koizumi, H., Mayanagi, Y., 2000. Noninvasive cerebral blood volume measurement during seizures using multichannel near infrared spectroscopic topography. J. Biomed. Opt. 5 (3), 287–290.

Wyatt, J.S., Cope, M., Delpy, D.T., Richardson, C.E., Edwards, A.D., Wray, S., Reynolds, E.O.R., 1990. Quantitation of cerebral blood volume in human infants by near-infrared spectroscopy. J. Appl. Physiol. 68, 1086–1091.

Yamashita, Y., Oda, M., Ohmae, E., Tamura, M., 1998. Continuous measurement of oxy- and deoxyhemoglobin of piglet brain by time-resolved spectroscopy. OSA TOPS 22, 205–207.

Zhang, H., Miwa, M., Urakami, T., Yamashita, Y., Tsuchiya, Y., 1998. Simple subtraction method for determining the mean path length traveled by photons in turbid media. Jpn. J. Appl. Phys. 37, 700–704.

Hum Genet (2005) 116: 340–346
DOI 10.1007/s00439-004-1232-5

ORIGINAL INVESTIGATION

Yoko Kawai · Akihiko Moriyama · Kiyofumi Asai
Carrie M. Coleman-Campbell · Satoshi Sumi
Hideko Morishita · Mariko Suchi

Molecular characterization of histidinemia: identification of four missense mutations in the histidase gene

Received: 7 October 2004 / Accepted: 8 November 2004 / Published online: 27 January 2005

Abstract Histidinemia (MIM235800) is characterized by elevated histidine in body fluids and decreased urocanic acid in blood and skin and results from histidase (histidine ammonia lyase, EC 4.3.1.3) deficiency. It is the most frequent inborn metabolic error in Japan. Although the original description included mental retardation and speech impairment, neonatal screening programs have identified the majority of histidinemic patients with normal intelligence. Molecular characteristics of histidase in histidinemia have not been determined, and cytogenetically visible deletions of 12q22-24.1 in which histidase gene resides have not been identified in histidinemic patients. In order to investigate whether individuals with this disorder have small deletions, additions, or point mutations in the histidase gene, we screened genomic DNA isolated from 50 histidinemic individuals who were discovered by the neonatal screening program. The methods employed included polymerase chain reaction (PCR) amplification of exons 1–21 of the histidase gene, followed by mutation detection enhancement gel electrophoresis and sequencing of the PCR products displaying heteroduplex bands. Four missense mutations (R322P, P259L, R206T, and R208L), two exonic polymorphisms (T141T c.423A → T and P259P c.777A → G), and two intronic polymorphisms (IVS6−5T → C and IVS9+25A → G) were identified. The frequencies of each polymorphism estimated either by dot blot allele-specific oligonucleotide hybridization, restriction enzyme digestion, or direct sequencing of the PCR products amplified from 50 unrelated normal individuals were 0.28, 0.30, 0.40, and less than 0.01, respectively. Mutation analysis of one family demonstrated that the patient inherited R322P from the mother and P259L from the father. This report describes the first mutations occurring in the coding region of the histidase structural gene in patients with histidinemia.

Y. Kawai
Pediatric Nursing, Nagoya City University School of Nursing, Nagoya, Japan

A. Moriyama
Graduate School of Natural Sciences, Nagoya City University, Nagoya, Japan

K. Asai
Department of Molecular Neurobiology, Graduate School of Medical Sciences, Nagoya City University, Nagoya, Japan

S. Sumi · H. Morishita · M. Suchi
Department of Pediatrics, Neonatology and Congenital Disorders, Graduate School of Medical Sciences, Nagoya City University, Nagoya, Japan

C. M. Coleman-Campbell
The General Clinical Research Center, The Children's Hospital of Philadelphia, Philadelphia, PA, USA

M. Suchi (✉)
Department of Pathology and Laboratory Medicine, The Children's Hospital of Philadelphia, University of Pennsylvania School of Medicine, Main Building 5203, 34th Street and Civic Center Boulevard, Philadelphia, PA 19104, USA
E-mail: suchi@email.chop.edu
Tel.: +1-215-5901728
Fax: +1-215-5901736

Introduction

Histidinemia (MIM 235800) is an autosomal recessive disorder resulting from histidase deficiency. Histidase (histidine ammonia lyase, EC 4.3.1.3) catalyses the non-oxidative deamination of histidine to urocanic acid, the first step in the major catabolic pathway of histidine (Taylor et al. 1991b). The metabolic blockade of histidase activity is associated with elevated histidine in body fluids and with decreased urocanic acid in blood and skin (Levy et al. 1995).

Most histidinemic children manifested with clinical abnormalities before the introduction of newborn screening programs in the 1970s. Screening programs

have altered this view substantially by identifying an asymptomatic majority population (Tada et al. 1984). Subsequent analyses, undertaken to evaluate relationships among histidinemia, mental retardation, and speech disturbances, suggest that histidinemia is a generally benign disorder (Scriver and Levy 1983; Tada et al. 1982). This view led to the decision to discontinue newborn screening for this disorder in 1992 in Japan. Few new cases have been diagnosed since the cessation of the screening, although histidinemia is the most frequent (1:8400) of inborn metabolic error in the Japanese population. We have been following 50 patients with abnormal serum histidine levels detected by the neonatal screening program since the initiation of the program in 1977. Our observations, including thorough developmental and pediatric psychiatric analyses, favor the view that histidinemia is a risk factor for the development of behavioral disorders, including learning disabilities, in individuals under specific circumstances such as abnormal perinatal events (Ishikawa 1987).

A molecular approach to this disorder may provide insights into the explanation for the diverse phenotypes of this disease, ranging from the minority of symptomatic patients to the majority who present few or no distinguishing clinical features. The human histidase gene (HAL) has been assigned to chromosome 12q22-12q24.1 (Taylor et al. 1991a). Attempts to identify cytogenetic abnormalities within this region among patients with histidinemia have been unsuccessful, and to this date, no cases with visible deletions of part of the region 12q22-24.1 have been documented with a deletion of the histidase gene locus. In a preliminary study of 17 histidinemia patients described in a review by Levy et al. (2001), a partial deletion or rearrangement of the histidase gene in a patient with normal intelligence was identified using a human histidase cDNA probe. However, there were no gross rearrangements in any other subjects.

In our laboratory, we have isolated and cloned cDNA and genomic DNA encoding human histidase (Suchi et al. 1993, 1995). In order to evaluate whether decreased histidase activity is caused by smaller histidase gene abnormalities, we screened 50 histidinemic patients for the presence of small deletions, additions, splice site mutations, or point mutations by mutation detection enhancement (MDE) gel analysis. We report here the identification of four missense mutations and two exonic and two intronic polymorphisms. These are the first mutations in the coding regions of the histidase gene described in patients with histidinemia.

Materials and methods

Subjects

Fifty patients detected as having high histidine levels by the neonatal screening program from 1977 to 1991 have been followed periodically at Nagoya City University Hospital. Serum histidine levels varied among the patients. One patient's highest recorded serum histidine level was 4.9 mg/dl at 1 month of age, although the Guthrie screening value was greater than 6 mg/dl. The highest serum histidine values during the follow-up of the remaining 49 patients were from 6.9 to 17.3 mg/dl (mean 12.1 ± 2.5 mg/dl). Twenty patients were given low histidine formula for variable lengths of time. None are currently receiving low histidine formula or on a restriction diet. Normal control subjects were unrelated and did not have any family history of inborn errors of metabolism.

Mutation detection and sequence analysis

Peripheral leukocyte genomic DNA was isolated as described (Baas et al. 1984) from 50 patients, selected family members of patients nos. 3 and 45, and 50 unrelated healthy Japanese individuals following informed consent.

Exons 1–21 and the flanking sequences of the histidase gene were amplified by polymerase chain reaction (PCR; Saiki et al. 1988). The DNA sequence of the histidase gene was obtained from a nucleotides site (http://www.ncbi.nlm.nih.gov/entrez/query.fcgi/nucleotide; accession nos. AB042205–AB042217). Oligonucleotide sequences and thermocycling conditions used in these amplifications are provided in Table 1. The goal was to include all *cis*-acting elements that participate in pre-mRNA splicing. To this end, the 3′-ends of all primers were designed to be located at least 42 base pairs (bp) away from the splice junctions. For the amplification and screening of exon 9, primers were selected not to include the 4-bp repetitive element in intron 8, 65 bp upstream from the intron–exon junction (Maffei et al. 1997).

MDE gels (AT Biochem, Malvern, Pa., USA) were used to analyze PCR products for the presence of small mutations in the histidase gene. Aliquots of 15 µl PCR product were combined with 3 µl loading dye (50% [w/v] sucrose, 0.6% [w/v] bromophenol blue, and 0.6% [w/v] xylene cyanol). The samples were heated at 95°C for 3 min, slowly cooled to 37°C, and run on 0.5×MDE gels containing 0.6×Tris-borate-EDTA (TBE) buffer (1×TBE = 0.089 M TRIS-borate, 0.002 M EDTA, pH 8.3). Gels were run overnight in 0.6×TBE at 20 V/cm for 12–18 h, depending on the size of the PCR product. MDE gels were stained for 15 min at room temperature in 1 µg/ml ethidium bromide in 0.6×TBE. Bands were visualized on a UV-*trans*-illuminator and photodocumented. In order to detect homozygous mutations, a second MDE gel analysis was performed on the PCRs mixed at a 10:1 ratio with the PCR product of the same region amplified from cloned histidase gene plasmids (Suchi et al. 1995).

Mutations were characterized by nucleotide sequencing whenever a heteroduplex band was detected. PCR-amplified products were subcloned into pCRII

Table 1 Histidase gene (HAL) primers and conditions for PCR amplification

Exons	Primer sequences Forward (5′–3′)Reverse (5′–3′)	Position	Annealing temperature (°C)
1	TCTCTGGCCTTTGCAGTCTTTTATGCAGAAGTG-GCTACC	−223* to c.−50 (exon 2)	54
2	AAGTGGACAGGAGGCT-CACGGGTTCAATGCTGCAAAGAC	c.−157 (exon 1) to IVS2+71	57
3, 4	GA-ACATGGCTGTACAATGTGCCCTGTTCTCCTTGA-CAGTG	IVS2−52 to IVS4+106	55
5, 6	TCAAGCTGTTCAGACTCACTTTATGATGCTATC-TATGACC	IVS4−42 to c.472 (exon 6)	53
6, 7	CCGTGGAAGTCTTTAACGTGAAGCCT-CATCCTCTGATCTG	IVS5−46 to IVS7+114	55
7, 8	AAATCCCTGCATTTAATTGCGGATAACTCA-CACTGTGCTG	IVS6−42 to IVS8+75	54
9	GGAGTTTGCTTTTCTTGGAATT-TCCCACTCATTTCAATT	IVS8−43 to IVS9+126	51
10	ACTCACTGGCAAAGCAAGGATAC-GAAGCATGCAAGCACAG	IVS9−70 to IVS10+73	54
11	GTTCCTGTAGGTCTCATTTCAAGGAATGATTG-AGGCTGAGA	IVS10−131 to IVS11+90	53
12	CGGGTATGTAGGTTCGTTACGTCTAAAGATCT-CAGCCACC	IVS11−59 to IVS12+76	55
13, 14	AAGGTAGGAGGATCGCT-AGATTTCATCCTGAACCTGGGGA	IVS12−124 to IVS14+74	55
15	TATTGGTACTCTTCAGGTAATCGAG-CAATGGAACTGAGAAGC	IVS14−58 to IVS15+103	54
16, 17	TCTCTTGCAGGAAGACTTGTCTGATTGCAGCA-AGTTCATG	IVS15−144 to c.1400 (exon17)	56
17	AACTGCTCTTGACCCAGAAGGAAAGACCCTTA-GATGGACG	IVS16−63 to IVS17+54	55
18	TCTGGAGAGTGTATCC-CATGGTTTCCAGGTGATGCTGATG	IVS17−106 to IVS19+103	56
19, 20	CAT-CTGTTAGTTGGGTGGTGCTGTGGGCTGCCTC-GATGT	IVS18−105 to c.1814 (exon 20)	58
20	ATCGCTTCATGGCCCCG-GACGGTGCACTTAGTGTTTATTA	c.1778 (exon 20) to IVS20+181	51
21	ACA-GCAGCTGTGTCTGGTCATGCCATCAGCCTAAC-CAACG	IVS20−119 to c.2125 (exon 21)	55

vector (TA cloning kit, Invitrogen, Carlsbad, Calif., USA). Nucleotide sequence information was determined by means of a Thermo sequence fluorescent labeled primer cycle sequencing kit (Amersham, Piscataway, N.J., USA) and an automatic A.L.F. red sequencing apparatus (Pharmacia, Peapack, N.J., USA). Base changes detected by sequencing were confirmed by either allele-specific oligonucleotide hybridization or restriction enzyme digestion. At least three clones from at least two separate PCRs were sequenced to verify newly identified base changes.

Allele frequencies

The frequency of two putative missense mutations (R322P and P259L) and a base change associated with a possible polymorphism, P259P (c.777A → G), was assessed by dot blot allele-specific oligonucleotide hybridization. Regions spanning exons 10 and 12 were amplified from genomic DNA samples of 50 normal unrelated individuals. PCR products (10 µl) were mixed with an equal volume of 4×SSC (1×SSC = 150 mM NaCl, 15 mM sodium citrate, pH 7.0) and heat-denatured at 95°C for 5 min. The denatured samples were blotted to Hybond-N+ nucleic acid transfer membrane (Amersham) via a Bio-Dot apparatus (BioRad, Hercules, Calif., USA). Filters were hybridized with allele-specific oligonucleotides labeled with [γ-32P]-ATP (>5,000 Ci/ml; Amersham) and T4 polynucleotide kinase (Takara Shuzo, Otsu, Shiga, Japan). The allele-specific oligonucleotides were 5′TTGCCCCACTCT-CTCAT3′, 5′TTGCCCTGCTCTCTCAT3′, and 5′TTGCCCCGCTCTCTCAT3′ for 259P, 259L, and 259P (c.777A → G), respectively, and 5′TGTA-GAGCGAGCCAGTG3′ and 5′TGTAGAGCCAG-CCAGTG3′ for 322R and 322P, respectively. Hybridizations and washes were according to the

standard procedure, and the hybridization results were visualized by autoradiographic exposure to New RX Medical X-ray film (Fuji, Tokyo, Japan).

Direct sequencing of the PCR products was employed to calculate the allele frequencies of two other putative missense mutations in exon 9 (R206T and R208L) and another intronic base change in intron 6 (IVS6−5 T → C). The PCR primers used were 5′ CCGTGGAAGTCTTTAACGTG3′ and 5′AAGCCTCATCCTCTGATCTG3′ for intron 6, and 5′GGGCTCAGACAAGTCAGACAG3′ and 5′CTTCTCAGGTGATTCCTCAGC3′ for exon 9 amplification. The latter pair of primers was also used for the direct sequencing of the PCR products from the parents of patient no. 45. The PCRs were purified by the Qiagen PCR purification kit (Qiagen, Valencia, Calif., USA) and sequenced using Big Dye Terminator v3.1 Cycle Sequencing kit (Applied Biosystems, Foster City, Calaif., USA).

Two other putative polymorphisms, T141T (c.423A → T) and IVS9+25T → C, involve restriction enzyme sites *Pvu*II and *Ava*II, respectively. T141T (c.423A → T) abolishes the *Pvu*II site, and IVS9+23T → C creates a new *Ava*II site. The frequency of these sequence variations was estimated utilizing these restriction sites. PCR-amplified DNA fragments from 50 normal unrelated individuals were purified using the PCR Purification kit, digested by 10 units of *Pvu*II or *Ava*II (New England Biolabs, Beverly, Mass., USA), and separated by electrophoresis in 1.2% agarose gels. The PCR primers were the same sets used to amplify intron 6 and exon 9 (see above) for T141T (c.423A → T) and IVS9+25T → C, respectively.

Results

MDE gel electrophoresis of PCR products spanning exons 6, 9, 10, and 12 revealed two to three bands in five, six, one, and one patient(s), respectively. Sequence analysis of these PCR products identified four missense mutations, two exonic base changes without amino acid changes, and two intronic base changes. These were: P259L (c.776CA → TG), P259P (c.777A → G), R322P (c.965G → C) in patient no. 3, R206T (c.617G → C) in patient nos. 12, 25, and 45, R208L (c.623G → T) in patient no. 44, T141T (c.423A → T) in patients nos. 6, 9, and 11, IVS6−5T → C in patient nos. 3, 6, 9,11, and 44, and IVS9+25A → G in patient nos. 17 and 28. Characteristics of these base changes are summarized in Table 2.

Patients 6, 9, and 11 harbored a silent base change T141T (c.423A → T) and an intronic sequence variation IVS6−5T → C. From each individual, at least five independent clones from at least two independent PCRs had this allele, whereas at least two clones had the same sequence as the reported histidase sequence. The latter intronic variation was also found in two other unrelated histidinemia patients (nos. 3 and 44) and was considered to be a polymorphism. Direct sequencing of PCR products from 50 unrelated normal individual demonstrated the frequency of IVS6−5T → C to be 0.40. As patients 6 and 9 are sister and brother, and as patient 11 is their cousin, T141T could have been a family-specific sequence. However, when *Pvu*II restriction enzyme digestion was applied to the PCR products from 50 normal individuals, it revealed that the frequency of T141T (c.423A → T) was 0.28 in this population.

In patient 3, three base changes were identified in exons 10 and 12. At codon 322 in exon 12, five of eight subclones had the sequence of CCA, which altered the amino acid arginine to proline (R322P), whereas the other three were CGA (Fig. 1). At codon 259 in exon 10, four of seven subclones had CTG, which codes for leucine (P259L), whereas the other three clones were CCG (P259P (c.777A → G)), which did not change the amino acid (proline) but was one base different from the reported CCA (Fig. 2). Sequence analysis and dot blot allele-specific hybridization of PCR products spanning exons 10 and 12 of the histidase genomic DNA of the parents revealed that the mother possessed a normal proline at amino acid 259 (259P/P259P(c.777A → G)) and was heterozygous for R322P, while the father had the normal 322R and was heterozygous for P259L/P259P (c.777A → G) (Fig. 3). The frequency of the polymorphism at codon 259 was estimated to be 0.30 by dot blot allele-specific oligonucleotide hybridization of 50 normal individuals (data not shown). R322P or P259L sequences were not detected in any of the 50 normal individuals by dot blot hybridization.

Table 2 Histidase mutations (*ASO* allele-specific oligonucleotide hybridization, *NA* not applicable)

Nucleotide change	Amino acid change	Position	Methods	Frequency
c.423A → T	T141T	Exon 6	*Pvu*II digestion	0.28
IVS6−5T → C	–	Intron 6	Direct sequencing	0.40
c.617G → C	R206T	Exon 9	Direct sequencing	NA
c.623G → T	R208L	Exon 9	Direct sequencing	NA
IVS9+25A → G	–	Intron 9	*Ava*II digestion	<0.01
c.776CA → TG	P259L	Exon 10	ASO	NA
c.777A → G	P259P	Exon 10	ASO	0.30
c.965G → C	R322P	Exon 12	ASO	NA

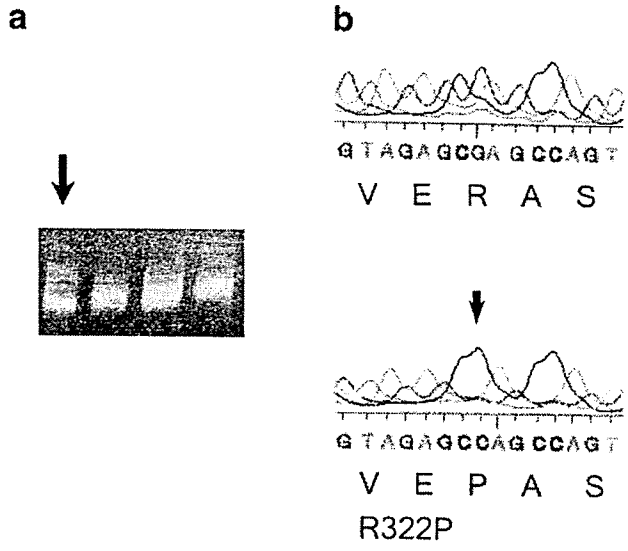

Fig. 1 **a** Mutation detection enhancement (MDE) gel electrophoresis of histidase exon 12 (*arrow* heteroduplex bands from patient no. 3).**b** Fluorescent dideoxy sequence analysis of exon 12. *Top* Normal reported sequence. *Bottom* A subcloned PCR product amplified from patient no. 3

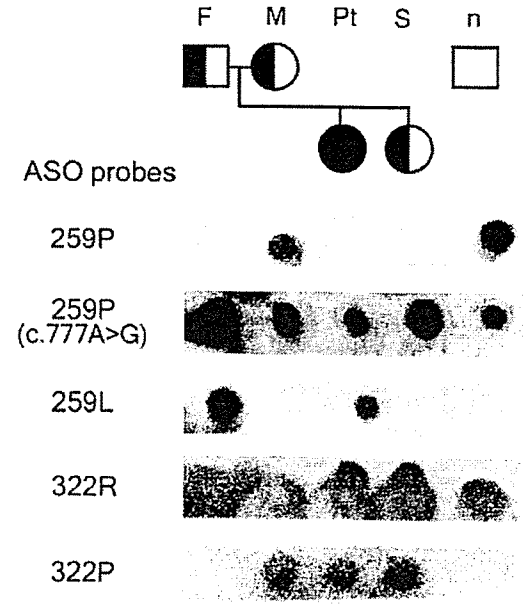

Fig. 3 Allele-specific oligonucleotide (*ASO*) hybridization analysis of PCR-amplified genomic DNAs from family members of patient no. 3 (*F* father, *M* mother, *Pt* patient, *S* sister, *n* unrelated control, *259P, 322R* probes from normal sequences, *259L, 322P* probes containing mutations, *259P (c.777A > G)* polymorphic sequence)

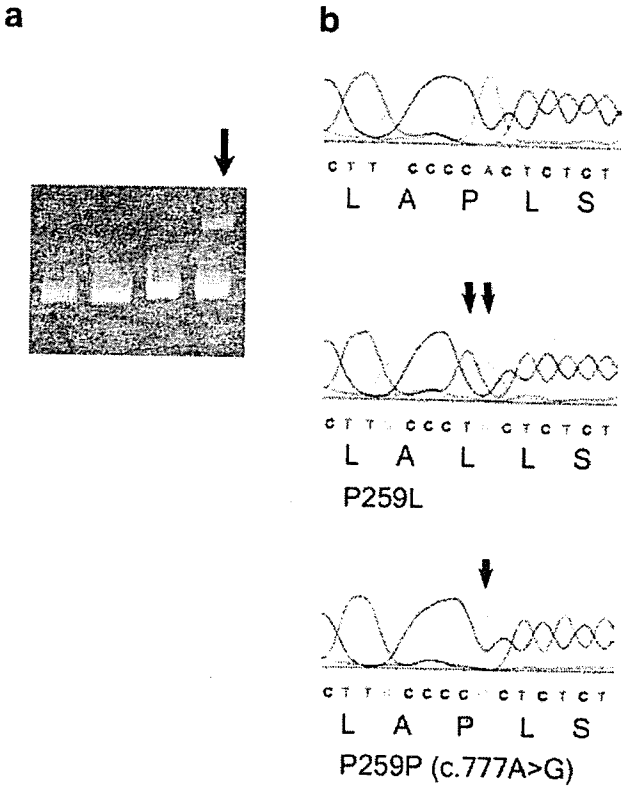

Fig. 2 **a** MDE gel electrophoresis of histidase exon 10 (*arrow* heteroduplex bands from patient no. 3). **b** Fluorescent dideoxy sequence analysis of exon 10. *Top* Normal reported sequence. *Middle* One of the subcloned PCR products amplified from patient no. 3. *Bottom* Another subclone

A missense mutation (R206T) was identified in exon 9 of patients 12, 25, and 45 (Fig. 4). At least three clones from each individual showed c.617G → C, while there were at least two clones with the normal sequence. No other mutation was detected in the other exons by MDE analysis in these patients. No R206T base change was detected in 50 normal individuals by direct sequencing of the region. Genomic DNA of the parents of patient no. 45 was obtained. Direct sequencing of the exon 9 region demonstrated the R208T sequence in the father who was heterozygous for this mutation.

An R208L missense mutation was identified in six subclones from two independent PCRs from one patient (no. 44), only six base pairs 3′ to the R206T mutation (Fig. 4). Two clones from the same PCR showed the normal sequence. Except for the presence of the aforementioned IVS6−5T → C, no other heteroduplex bands were detected in the histidase gene from this patient. Direct sequencing demonstrated that this base change was not present in 50 normal individuals.

Two other unrelated patients (nos. 17 and 28) who displayed heteroduplex bands in the exon 9 region had an intronic sequence variation, IVS9+25A → G. One of 50 normal individuals was revealed to harbor this base change by PCR amplification and *Ava*II restriction digestion. This normal individual was also heterozygous for IVS9+25A → G. Three additional normal individuals were assayed for this base change; no PCR segments were digested by *Ava*II.

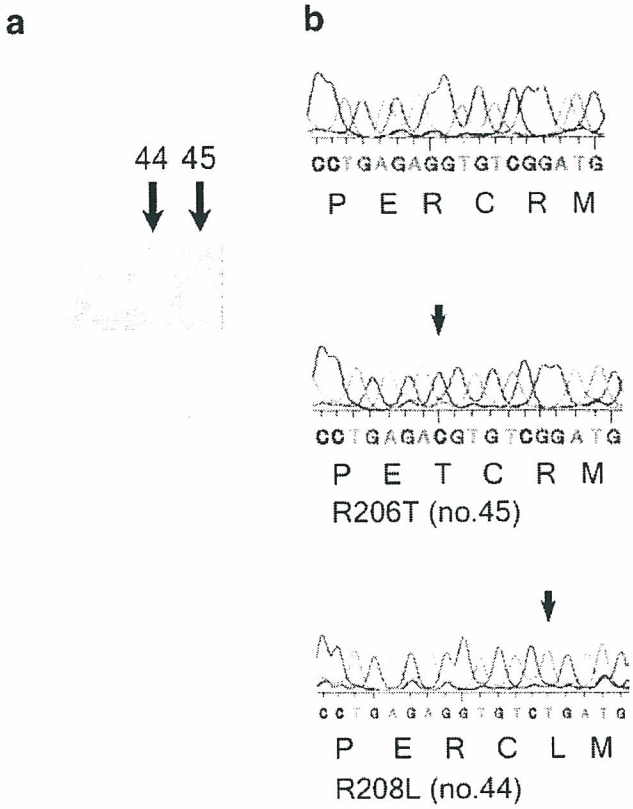

Fig. 4 **a** MDE gel electrophoresis of histidase exon 9 (*arrows* heteroduplex bands from patient nos. 44 and 45). **b** Fluorescent dideoxy sequence analysis of exon 9. *Top* Normal reported sequence. *Middle* A subcloned PCR product amplified from patient no. 45. *Bottom* A subcloned PCR product amplified from patient no. 44

Discussion

Histidinemia is an autosomal recessive amino acid metabolism disorder in which the patients have decreased histidase activity in the liver and epidermal stratum corneum (Levy 1988). Mammalian histidase has a molecular mass of about 200 kDa and is described to consist of three identical subunits of 75 kDa each (Okamura et al. 1974; Taylor et al. 1990). Several genetic mechanisms can be considered to cause the deficiency in an enzyme composed of a homotriplex: (1) a large deletion of the gene, either cytogenetically visible and spanning several other genes or detectable by Southern blot analysis, (2) an aberration in the *cis*-element sequence, such as promoter and enhancer regions, (3) a coding sequence abnormality or intronic sequence abnormality that results in qualitatively or quantitatively abnormal mRNA, (4) abnormalities in post-translational modification, and (5) abnormalities in regulatory proteins. Some cases of histidinemia involving mental retardation or other abnormalities might result from a contiguous gene syndrome in which the HAL locus and genes adjacent to it are deleted. However, no cases with a HAL locus deletion have been demonstrated among patients with histidinemia or those with translocations of 12q or deletions in 12q (Levy et al. 2001).

In this report, we have focused on the hypothesis that histidase activity is reduced in patients with histidinemia because of mRNA abnormality. There are suggestions, in at least some patients, that mutations have occurred in the coding region of the histidase structural gene. Kuroda et al. (1982) have demonstrated an altered sensitivity of skin histidase to denaturation in two patients. To investigate this possibility by molecular techniques, we screened histidase genomic DNA for mutations.

Two missense mutations R322P and P259L were identified in exons 12 and 10, respectively, in one patient, no. 3. Dot blot allele-specific oligonucleotide hybridization and sequence analysis of the respective exons revealed that R322P was inherited from the mother and P259L from the father. Both codons are conserved among mouse, rat, and human. R322P changes the basic amino acid to neutral proline. Taylor et al. (1993) have reported an R322Q mutation in a histidinemic mice population. The R322Q mutation in the mouse is expressed in Cos1 cells and has been demonstrated to have decreased histidase activity compared with the enzyme protein with the wild-type arginine at codon 322. P259L also involves the amino acid proline and possibly affects the secondary structure of the polypeptide. The mutation R206T was found in three unrelated histidinemia patients (nos. 12, 25, and 45). Only one patient (no. 44) possessed the R208L mutation, which lies 6 bp 3′ to the R206T mutation. The two arginines, one amino acid apart, are expected to create a strong negative charge in this portion of the polypeptide, and a change to a neutral amino acid in one of these arginines could cause a major conformational alteration in the enzyme protein. Although the effect of these missense mutations on the activity of histidase has not been demonstrated in vitro, all of the base changes lead to nonconservative amino acid substitutions. In addition, these four changes have not been identified in 100 alleles of 50 normal individuals by dot blot hybridization or by direct sequencing, providing additional support that they are disease-causing mutations.

Two intronic sequence variations were also identified within the histidase gene during this study. Both occurred in more than one patient. One of them, IVS9+25A → G, was present in one of 106 alleles from normal individuals. With the incidence of histidinemia among Japanese being 1:8400, one in 46.3 people is expected to be a heterozygous carrier. It is still possible that IVS9+25A → G is a disease-causing base change, however, it is less likely to cause abnormal splicing in the transcribed RNA, because the base change is more than 20 bp away from the intron–exon junctions. The second intronic base change, IVS6−5T → C, is at a −5 position in the respective intron and may affect splicing efficiency. However this base change is seen in normal individuals

with a frequency of 0.40 by PCR amplification and subsequent direct sequencing.

One of the two exonic polymorphisms P259P (c.777A → G) occurs in the normal population with the frequency of 0.30. The polymorphic P259P (c.777A → G) at codon 259 was identified in five of six alleles in the family members of patient no. 3 excluding the alleles with P259L. Although the reported "normal" codon 259 is CCA, the mutated sequence CTG is likely to have arisen from CCG with the second C changing to T, rather than via two base changes from CCA.

MDE analysis yielded no heteroduplex bands in a number of amplified exonic regions. Several reasons for the low sensitivity of heteroduplex occurrence can be proposed. One is that a true false-negative might occur in which the MDE gel does not produce heteroduplex bands even when there is a mismatch in the strands of the amplified DNA. False-negative rates are reported to vary depending on the length of the PCR products. Another reason is that, if there is a deletion of the gene or part of the gene in one allele, PCR will only amplify the remaining normal allele, resulting in one band. In addition, when a mutation resides at a point at which PCR primers anneal, the allele containing the mutation will not be amplified. The strategy that we have adapted will also miss 5′ promoter mutations and large intronic deletions that may alter transcription efficiency, RNA stability, or splicing. Moreover, histidinemia, despite a consistent biochemical phenotype, may include more than one form of histidase deficiency, namely a more frequent benign type and a less frequent maladaptive variant. One form could arise because of an abnormality in a protein other than histidase protein, such as one of the regulatory proteins. Lastly, one case in this series demonstrated serum histidine levels at a high normal range despite Guthrie's test results showing a value greater than 6 mg/dl. Determination of histidase activity levels will thus be necessary to confirm the diagnosis of histidinemia.

In summary, four missense mutations have been identified within the histidase gene among 50 patients with abnormal histidine levels detected through the newborn screening program. This is the first report in which mutations have been documented within the coding region of this gene.

Acknowledgments We thank the late Dr. Taiji Kato for graciously providing access to his laboratory facilities in the Department of Molecular Neurobiology, Drs. Yoshiro Wada and Hisako Saito for their seminal work and continuous encouragement, Dr. Haruo Mizuno for the preparation of genomic DNA from normal individuals, and Manami Yamamoto for her technical assistance. We are also grateful to physicians in the Department of Pediatrics, Neonatology and Congenital Disorders, Nagoya City University for the care of the patients and to laboratory staff members of the General Clinical Research Center, The Children's Hospital of Philadelphia for their technical support. This study was supported in part by a Research Grant from the Ministry of Health, Labor, and Welfare of Japan and NIH/NRCC grant M01-RR00240.

References

Baas F, Bikker H, Ommen E-JB van, Vijlder JJM de (1984) Unusual scarcity of restriction site polymorphism in the human thyroglobulin gene: a linkage study suggesting autosomal dominance of a defective thyroglobulin allele. Hum Genet 67:301–305

Ishikawa M (1987) Developmental disorders in histidinemia—follow-up study of language development in histidinemia. Acta Paediatr Jpn 29:224–228

Kuroda Y, Watanabe T, Ito M, Toshima K, Miyao M (1982) Altered kinetic properties of skin histidase in two patients with histidinaemia. J Inherit Metab Dis 5:73

Levy HL (1988) Disorders of histidine metabolism. In: Scriver CR, Beardet AL, Sly WS, Valle D (eds) Metabolic basis of inherited disease, 6th edn. McGraw-Hill, New York, pp 563–576

Levy HL, Taylor RG, McInnes RR (1995) Disorders of histidine metabolism. In: Scriver CR, Beardet AL, Sly WS, Valle D (eds) The metabolic and molecular bases of inherited disease, 7th edn. McGraw-Hill, New York, pp 1107–1123

Levy HL, Taylor RG, McInnes RR (2001) Disorders of histidine metabolism. In: Scriver CR, Beardet AL, Sly WS, Valle D (eds) The metabolic and molecular bases of inherited disease. McGraw-Hill, New York, pp 1807–1820

Maffei P, Nobile M, Di Bella D, Novelli E, Smeraldi E, Catalano M (1997) Intragenic tetranucleotide repeat polymorphism at the human histidase (HAL) locus. Clinical Genet 52:194–195

Okamura H, Nishida T, Nakagawa H (1974) L-histidine ammonia-lyase in rat liver. I. Purification and general characteristics. J Biochem (Tokyo) 75:139–152

Saiki RK, Gelfand DH, Stoffel S, Scharf SJ, Higuchi R, Horn GT, Mullis KB, Erlich HA (1988) Primer-directed enzymatic amplification of DNA with a thermostable DNA polymerase. Science 239:487–491

Scriver CR, Levy HL (1983) Histidinaemia. Part I: reconciling retrospective and prospective findings. J Inherit Metab Dis 6:51–53

Suchi M, Harada N, Wada Y, Takagi Y (1993) Molecular cloning of a cDNA encoding human histidase. Biochim Biophys Acta 1216:293–295

Suchi M, Sano H, Mizuno H, Wada Y (1995) Molecular cloning and structural characterization of the human histidase gene (HAL). Genomics 29:98–104

Tada K, Tateda H, Arashima S, Sakai K, Kitagawa T, Aoki K, Suwa S, Kawamura M, Oura T, Takesada M, Kuroda Y, Yamashita F, Matsuda I, Naruse H (1982) Intelectual development in patients with untreated histidinemia. J Pediatr 101:562–563

Tada K, Tateda H, Arashima S, Sakai K, Kitagawa T, Aoki K, Suwa S, Kawamura M, Oura T, Takesada M, Kuroda Y, Yamashita F, Matsuda I, Naruse H (1984) Follow-up study of a nation-wide neonatal metabolic screening program in Japan. Eur J Pediatr 142:204–207

Taylor RG, Lambert MA, Sexsmith E, Sadler SJ, Ray PN, Mahuran DJ, McInnes RR (1990) Cloning and expression of rat histidase. Homology to two bacterial histidases and four phenylalanine ammonia-lyases. J Biol Chem 265:18192–18199

Taylor RG, Garcia-Heras J, Sadler SJ, Lafreniere RG, Willard HF, Ledbetter DH, McInnes RR (1991a) Localization of histidase to human chromosome region 12q22–q24.1 and mouse chromosome region 10C2–D1. Cytogenet Cell Genet 56:178–181

Taylor RG, Levy HL, McInnes RR (1991b) Histidase and histidinemia. Clinical and molecular considerations. Mol Biol Med 8:101–116

Taylor RG, Grieco D, Clarke GA, McInnes RR, Taylor BA (1993) Identification of the mutation in murine histidinemia (his) and genetic mapping of the murine histidase locus (Hal) on chromosome 10. Genomics 16:231–240

J Hum Genet (2006) 51:518–522
DOI 10.1007/s10038-006-0392-7

ORIGINAL ARTICLE

Satoshi Sumi · Hiroko Taniai · Taishi Miyachi
Mitsuyo Tanemura

Sibling risk of pervasive developmental disorder estimated by means of an epidemiologic survey in Nagoya, Japan

Received: 21 December 2005 / Accepted: 14 February 2006 / Published online: 25 March 2006

Abstract Broad-spectrum autism, referred to as pervasive developmental disorder (PDD), may be associated with genetic factors. We examined 241 siblings in 269 Japanese families with affected children. The sibling incidence of PDD was 10.0% whereas the prevalence of PDD in the general population in the same geographic region was 2.1%. Both of these rates are higher than those reported previously, probably because of the expanded clinical criteria applied. The prevalence in males of the general population was 3.3% and that in females was 0.82%. The sibling incidences were 7.7 and 20.0% for families in which the probands were male and female, respectively. Because the reversed sex ratios correspond to the general rule for a multifactorial threshold model, we suggest that most PDD cases result from the cumulative effects of multiple factors (mostly genetic). The sibling incidences were 0 and 10.9% for families in which the proband had low and normal birth-weight, respectively, suggesting the risk is lower in families with low-birth-weight probands.

Keywords Autism · Pervasive developmental disorder · Sibling · Low birth-weight · Multifactorial inheritance

S. Sumi (✉)
West District Care Center for Disabled Children,
20-48 Komoto, Nakagawa-ku, Nagoya 454-0828, Japan
E-mail: satoshi-sumi@mbn.nifty.com
Tel.: +81-52-3619555
Fax: +81-52-3619560

H. Taniai
Department of Pediatrics, Neonatology and Congenital Disorders, Graduate School of Medical Science, Nagoya City University, Nagoya, Japan

T. Miyachi
Department of Pediatrics, Nagoya Child Welfare Center, Nagoya, Japan

M. Tanemura
Division of Clinical and Molecular Genetics, Nagoya City University Hospital, Nagoya, Japan

Introduction

Autism is a behaviorally defined syndrome, characterized by pervasive impairment of social interaction and communication and the presence of stereotypical characteristics. Although these clinical symptoms may arise from brain dysfunction, clinical severity is modified by environmental factors. In the past decade, criteria for diagnosis of autism have been expanded, from a strict category (Kanner type) to a broad spectrum, owing to progress in neuropsychological understanding (Wing 1996). The broad spectrum of autism is defined as pervasive developmental disorder (PDD) in the DSM-IV criteria (American Psychiatric Association 1994) and the number of cases has recently increased rapidly, in line with the expanding criteria. A recent study described the prevalence in the Japanese general population to be more than 1% (Honda et al. 2005).

Previous studies of twins have suggested that autism is strongly affected by genetic factors. Ritvo et al. (1985) found that the concordance for autism by pairs was 96% in 23 monozygotic twins and 24% in 17 dizygotic twins; Steffenburg et al. (1989) reported respective values of 91 and 0%. Bailey et al. (1995) reported concordance for classical autism to be 60% in monozygotic and 0% in dizygotic twins, but for the broad spectrum disease it was 92% and 10%, respectively. These results show that autism is strongly affected by genetic factors but is also affected by the environment. Previous sibling studies have also suggested genetic effect on autism, with August et al. (1981), Baird et al. (1985), Chakrabarti et al. (2001), and Icasiano et al. (2004) reporting sibling risks of 2.8, 5.9, 3.9, and 6.3%, respectively. These frequencies are much higher than that in the general population but

much lower than that in single-gene diseases. As far as we are aware, all previous studies involving both twins and siblings were performed on Caucasian populations only. Several genome-wide investigations have proposed susceptibility loci associated with autism (PDD), but neither a single candidate gene nor an inheritance mode for autism have been determined (Shastry 2003). It has also been suggested that PDD may be caused by non-genetic factors, for example neonatal factors.

In this study we estimated the prevalence of PDD in the general population of the western region of Nagoya, Japan, and examined the overall sibling incidence and the incidence after families were classified by the sex and birth-weight of the probands. We suggest a model for the etiology of PDD based on our results.

Subjects and methods

Screening and diagnosis

This study was conducted using a regional support system for children. The western region of Nagoya is a residential area with high population density—half a million people within 97 km^2. Infants with any developmental problems are detected by a screening system which is well organized by local government. The first stage of the system is a routine health check at general health centers; the average percentage attendance in 2001–2003 was 95.3 and 86.5% for 18-month-old and 3-year-old children. Pediatricians and public health nurses examine development and all infants with developmental problems (including mild symptoms) are referred to the West District Care Center for Disabled Children (WDC center). The second stage is based on observation at kindergartens and day nurseries. Psychologists from the WDC center make regular visits and refer cases to the WDC center when necessary. Because the number of infants attending kindergartens or nurseries is 99.7% in this area, most infants with problems should be noticed. The WDC center also cooperates with general hospitals in the area. Because there are no departments of pediatric psychiatry, children are always referred to the WDC center. Medical examinations such as chromosome analyses are performed at hospitals and the results are sent to the WDC center. On initial examination at the WDC center, psychologists obtain detailed histories from parents and also conducted an intelligence quotient test (Tanaka-Binet) on all children. In addition, pediatric psychiatrists observe children's behavior carefully in a play space with the help of public health nurses. If children have developmental problems, they start educational programs (group style or individual therapy) at the center. After repeated observation both by psychologists and pediatric psychiatrists, children are finally diagnosed, at the age of four or above, using the DSM-IV (American Psychiatric Association 1994) criteria.

In this study we excluded autistic children with certain disorders (two cases with Duchenne muscular dystrophy, two with Down syndrome, one with 18p partial monosomy, and one with tuberous sclerosis).

Prevalence and siblings

In this study we first estimated the prevalence of PDD in the general population. At the center we diagnosed 281 infants who were born between 1995 and 1999 as having PDD. The number of affected children (281) was divided by the total number of age-matched children residing in the area (13,568 children, consisting of 6,949 boys and 6,619 girls). The parents were all Japanese.

For the sibling study we excluded families with siblings younger than 4 years. This resulted in a cohort of 269 families whose characteristics are listed in Table 1. The affected siblings had already been diagnosed in our regional system before this study started. To avoid

Table 1 Characteristics of the families, probands, and siblings that formed the cohort of this study

Family factors	Number of families
All families	269
Children per family	
1 child	85
2 children	136
≥3 children	41
Average	1.9
Affected children per family	
1 child	247
2 children	22
≥3 children	1
Average	1.09
Proband factors	**Number of probands**
All probands	269
Male	215
Female	54
Sex ratio	3.98
Birth weight	
≥2,500	240
< 2,500	29
Detailed clinical criteria	
Autistic	77
PDD-NOS	119
Asperger	73
Sibling factors	**Number of siblings**
All siblings excluding probands	241
Unaffected siblings	217
Male	105
Female	112
Sex ratio	0.94
Affected siblings	24
Male	13
Female	11
Sex ratio	1.18

Autistic, autistic disorder; PDD-NOS, pervasive developmental disorder not otherwise specified; Asperger, Asperger's disorder

non-detection of autistic siblings, we interviewed parents again about the behavior of their children and made further examinations at the center if they showed even minor problems. This procedure did not identify any new affected siblings. We indicate the firstborn PDD as the proband in multiple incidence families. The sibling risk (concordance rate) was determined as the number of PDD siblings divided by the total number of siblings.

Results

In the general population the prevalence of PDD was 2.1% (281/13,558), 3.3% (227/6,949) for boys and 0.82% (54/6,619) for girls. In the sibling study 23 multiple-incidence families were found as shown in Fig. 1. There were only two families (families 1 and 2) with further births after two affected children, but in family 1 the third child was also affected. Table 2 lists the incidence (concordance rate) among siblings. The incidence of PDD in all siblings was 10.0%, with values of 7.7 and 20.0% for families in which the probands were male and female, respectively. The incidences were 0 and 10.9% for families in which the probands had low and normal birth-weight, respectively.

Discussion

Pervasive developmental disorder, including classical autism, has received much attention in recent decades, especially because the criteria for clinical diagnosis of autism have been expanded from strict categorization to a broad spectrum. PDD is manifested by a difficulty in social communication, but the detailed etiology remains unclear. Although PDD (autism) seems to be strongly affected by genetic factors, several genome-wide investigations have failed to determine a single candidate gene, suggesting that several genes may be associated with this disorder.

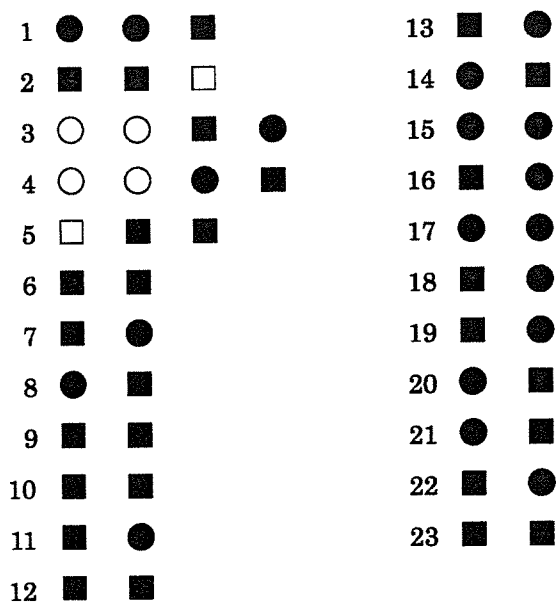

Fig. 1 Birth order of PDD probands and their siblings in 23 families with multiple affected children: *filled square*, male with PDD; *filled circle*, female with PDD; *open square*, normal male; *open circle*, normal female

In this study sibling incidence was 10.0%, in contrast with 2.1% in the general population. Both values were higher than in a previous report using DSM-III criteria (American Psychiatric Association 1980). The differences presumably reflect our application of the DSM-IV criteria. We believe our results may be used in genetic counseling for Japanese families, but further data are necessary to establish better guidelines.

The sibling incidence may also provide evidence to judge the mode of inheritance. It is unlikely that PDD has an autosomal dominant or an autosomal recessive mode of inheritance, because, theoretically, sibling incidence would then be 50 and 25%. In multifactorial inheritance, sibling incidence (Q) is estimated from the prevalence in general population (p): $Q=\sqrt{p}$ (Edwards' method; Emery 1986). Theoretical sibling incidence based on the prevalence in the population is 14.4%. Sibling incidence in our survey (10.0%) is therefore much closer to that for multifactorial inheritance mode than that for autosomal inheritance.

We examined the effect of sex on the incidence risk. The number of male probands was approximately four times that of female probands (Table 1). Sibling incidence for families with a male proband was less than half that for families with a female proband, however. The reversed sex ratios correspond to the general rule for a multifactorial threshold model (Carter 1969; Harper 2004), i.e. where there is unequal sex incidence, the risk is higher for relatives of a proband of the sex in which the condition is less common. A proband of the more rarely affected sex requires a greater genetic factor to develop the disorder. Such reversed sex ratios in autistic families were also observed by Ritvo et al. (1989). Other phenomena which corresponded to a multifactorial threshold model were also found in previous studies—a high sibling risk (35.3%) was noted in families with multiple affected children (Ritvo et al. 1989), with a wide discrepancy of risk between monozygotic and dizygotic twins (Ritvo et al. 1985; Steffenburg et al. 1989; Bailey et al. 1995).

X-linked recessive inheritance can be excluded using our data for prevalence in the general population. Because the prevalence in males was 3.3%, the expected frequency of affected females (assuming Hardy–Weinberg equilibrium) is the square of this number, 0.11%. The actual observed prevalence in females was 0.82%, however. If PDD had an X-linked dominant inheritance mode, the prevalence in females should be higher than in males. An imperfect X-linked dominant cannot, however, be excluded using the data for prevalence. It is, moreover, difficult to prove the mode of inheritance if several inheritance types are mixed or if non-genetic

Table 2 Incidence rates in siblings

Family category (Number of families)	Number of siblings and incidence rate			
	All siblings	Affected siblings	Incidence (%)	95% cl
All families [269]	241 (male 118, female123)	24 (male 13, female 11)	10.0 (male 11.0, female 8.9)	6.5–14.5 (6.0–18.1, 4.5–15.4)
Sex				
Families with male probands [219]	196	15	7.7	4.3–12.3
Families with female probands [50]	45	9	20.0	9.6–34.6
Birth-weight				
Families with NBW probands [240]	220	24	10.9	7.1–15.8
Families with LBW probands [29]	21	0	0.0	0.0

cl, confidence limits; NBW, normal birth weight; LBW, low birth weight

factors are mixed. A larger cohort is thus necessary for statistical examination and for drawing conclusions about the mode of inheritance.

Non-genetic factors have also come under consideration. A case control study showed that obstetric complications did not increase the risk of autism (Cryan et al.1996), but Indredavik et al. (2004) demonstrated that the rate of incidence with the Asperger syndrome was higher (4/56) than in controls (0/81). In this study sibling incidences were 0 and 10.9% for families in which the proband had low or normal birth-weight, respectively. Although there were few low-birth-weight siblings, this suggests the risk in families with low-birth-weight probands is lower.

Several models have been proposed for the etiology of PDD. Gillberg et al. (2000) described PDD (autism) to be a syndrome resulting from many individual diseases (factors), but this has been criticized by Jones et al. (2002), who proposed a risk factor model, supposing cumulative effects of multiple factors (mostly genes), in general agreement with a multifactorial threshold model.

Because our results for sibling incidence also provide support for such a model, we suggest that most PDD cases result from the cumulative effects of multiple factors (mostly genetic). Although there remains a possibility that one (or a few) major factor(s) could also cause PDD, this would not affect the results of our survey if the proportion were very small. Many factors, including single gene disorders and infection and neonatal factors, have been reported to be associated with PDD. For example, Jamain et al. (2003) suggested that defects in a single X-linked gene encoding neuroligin (cell-adhesion molecules at synapses) might cause autism. This needs to be taken into consideration in further investigations.

Finally we propose a model for the etiology for PDD encompassing two groups:

1 a large group in which the syndrome results from the cumulative effects of multiple factors (mostly genetic), namely a multifactorial disorder; and
2 a small group in which it results from separate individual factors.

This is in line with the classical model of Penrose (1963) who divided mental retardation into two groups:

1 a physiological group which is biased in the normal distribution for intelligence; and
2 a pathological group resulting from various kinds of neurological disease.

Further investigations of larger numbers of families, genes, and non-genetic factors are necessary for clarification.

References

American Psychiatric Association (1980) Diagnostic and statistical manual of mental disorders: DSM-III, 3rd edn. American Psychiatric Association, Washington DC

American Psychiatric Association (1994) Diagnostic and statistical manual of mental disorders: DSM-IV, 4th edn. American Psychiatric Association, Washington DC

August GJ, Stewart MA, Tsai L (1981) The incidence of cognitive disabilities in the siblings of autistic children. Br J Psychiatry 138:416–422

Bailey A, Le Counteur A, Gottesman I, Bolton P, Simonoff E, Yuzda E, Rutter M (1995) Autism as a strongly genetic disorder: evidence from a British twin study. Psychol Med 25:63–77

Baird TB, August GJ (1985) Familial heterogeneity in infantile autism. J Autism Dev Discord 15:315–321

Carter CO (1969) Genetics of common disorders. Br Med Bull 25:52–57

Chakrabarti S, Fombonne E (2001) Pervasive developmental disorders in preschool children. JAMA 27:3093–3099

Cryan E, Byrne M, O'Donovan A, O'Callaghan E (1996) A case study of obstetric complications and later autistic disorder. J Autism Dev Disord 26:453–460

Emery AEH (1986) Methodology in medical genetics, 2nd edn. Longman Group Ltd, Edinburgh

Gillberg C, Colman M (2000) The biology of the autistic syndromes 3rd edn. Mac Keith Press, London

Harper PS (2004) Practical genetic counselling, 6th edn. Oxford University Press, London

Honda H, Shimizu Y, Rutter M (2005) No effect of MMR withdrawal on the incidence of autism: a total population study. J Child Psychol Psychiatry 46:572–579

Indredavik MS, Vik T, Heyerdahl S, Kulseng S, Fayers P, Brubakk AM (2004) Psychiatric symptoms and disorders in adolescents with low birth weight. Arch Dis Child Fetal Neonatal Ed 89:445–450

Icasiano F, Hewson P, Machet P, Cooper C, Marchall A (2004) Childhood autism spectrum disorder in Barwon region: a community based study. J Paediatr Child Health 40:696–701

Jamain S, Quach H, Betancur C, Rastam M, Colineaux C, Gillberg IC (2003) Mutation of X-linked genes encoding neuroligins

NLGN3 and NLGN4 are associated with autism. Nat Genet 34:27–29
Jones MB, Szatmari P (2002) A risk factor model of epistatic interaction, focusing on autism. Am J Med Genet (Neuropsychiatr Genet) 114:558–565
Penrose LS (1963) The biology of mental defect. 3rd edn. Sidgwick and Jackson Ltd, London
Ritvo E, Freeman BJ, Manson-Brothers AMA, Ritvo AM (1985) Concordance for the syndrome of autism in 40 pairs of afflicted twins. Am J Psychiatry 142:74–77
Ritvo ER, Jorde LB, Manson-Brothers A, Freeman BJ, Pingree C, Marshall MS, Jones B, McMahon WM, Petersen BP, Jenson WR, Mo Amy (1989) The UCLA-university of Utah epidemiologic survey of autism: recurrence risk estimates and genetic counseling. Am J Psychiatry 146:1032–1036
Shastry BS (2003) Molecular genetics of autism spectrum disorders. J Hum Genet 48:495–501
Steffenburg S, Gillberg C, Hellgren L, Andersson L, Gillberg IC, Jakobsson G, Bohman M. (1989) A twin study of autism in Denmark, Finland, Iceland, Norway and Sweden. J Child Psychol Psychiatry 30:405–416
Wing L (1996) The autism spectrum. A guide for parents and professionals. Constable and Company Ltd, London

第93回日本小児精神神経学会
シンポジウム「子どものこころの臨床における発達について再考する」

自閉症臨床から

杉　山　登志郎*

Ⅰ．発達精神病理学とは何か

今回のシンポジウムのテーマである，自閉症のこころの臨床における発達というテーマを考察するうえで，精神病理学の重要性を最初に取り上げておきたい．

精神病理学(psychopathology)という学問は，今日ほとんど顧みられなくなった感があるが，本来は身体医学における病理学と同様，精神医学における臨床の基礎をなすものである．精神病理学には実は二つの意味がある．一つは，ほとんど症状学と同義語として用いられていて，精神科疾患のさまざまな症状に関しその概念を疾患ごとにまとめたものである．しかし真の意味は別にあり，一般的な心理学では届きにくい病的心理を扱う医学的心理学である(笠原，1987)．この領域の存在こそが，他の身体医学から精神医学を分ける独自の部分であり，いわゆるこころの臨床を特徴づけるものである．また逆に，こころの臨床に立ち入ることが可能か否かは，精神病理学の研鑽を積んでいるか否かによって分けられるといって過言ではない．身体科のみを基盤とする，こころの臨床における限界の大部分がこの点にあり，筆者としては発達障害における臨床も同一であると考える．

精神病理学の持つ意味を具体的な例で示してみよう．例えば幻覚，妄想が明らかな青年を前にすれば，医学教育課程を学んだすべての医師にとって統合失調症の診断を下すことは可能であろう．また精神科薬理学の知識を持つ医師であれば，適切な薬物療法の処方を行うことも可能である．しかしながら，統合失調症の患者に対し治療者として寄り添うためには，その患者がどのような内的世界にあるのかを知ることが必要不可欠となる．それは健常者にとって容易に理解ができる世界ではない．精神科疾患の一部の体験世界は，通常の常識的心理学では届かないからこそ，独自の医学的心理学を必要とするのである．統合失調症の患者が先へ先へと自分の存在を投企させようとしているとき，その焦りに共感しつつ治療者が掛けることばによってのみ，その激しい生き焦りを少しでも引き留めることが可能となるのであって，その内的な世界を無視した対応は極めて敏感な患者に対して侵襲的に作用こそすれ，治療的にはならないであろう(中井，1974)．このような体験世界を学んではじめて統合失調症者の持つ脆弱性の理解も可能となる．

このような問題はもっと一般的な，健常心理の近くにある現象についても事情は同じであ

Toshiro SUGIYAMA : The Case of Antism
*あいち小児保健医療総合センター［〒474-8710 大府市森岡町尾坂田 1-2］